Efficient Spin Injection into Graphene through a Tunnel Barrier: Overcoming the Spin-Conductance Mismatch

Qingyun Wu,[1] Lei Shen ((沈雷)),[2,1,*] Zhaoqiang Bai,[1] Minggang Zeng,[1] Ming Yang,[1] Zhigao Huang,[3] and Yuan Ping Feng[1,†]

[1]*Department of Physics, National University of Singapore, Singapore 117542, Singapore*
[2]*Engineering Science Programme, Faculty of Engineering, National University of Singapore, Singapore 117579, Singapore*
[3]*College of Physics and Energy, Fujian Normal University, Fuzhou 350007, People's Republic of China*

(Received 30 May 2014; revised manuscript received 30 August 2014; published 16 October 2014)

Employing first-principles calculations, we investigate the efficiency of spin injection from a ferromagnetic electrode (Ni) into graphene and a possible enhancement by using a barrier between the electrode and graphene. Three types of barriers, *h*-BN, Cu(111), and graphite, of various thickness (0–3 layers) are considered, and the electrically biased conductance of the Ni/barrier/graphene junction is calculated. It is found that the minority-spin-transport channel of graphene can be strongly suppressed by the insulating *h*-BN barrier, resulting in a high spin-injection efficiency. On the other hand, the calculated spin-injection efficiencies of Ni/Cu/graphene and Ni/graphite/graphene junctions are low, due to the spin-conductance mismatch. Further examination of the electronic structure of the system reveals that the high spin-injection efficiency in the presence of a tunnel barrier is due to its asymmetric effects on the two spin states of graphene.

DOI: 10.1103/PhysRevApplied.2.044008

I. INTRODUCTION

In the past decade, graphene has been the focus of intensive materials research due to its potential applications in many areas [1]. Because of the weak spin-orbital coupling in the carbon system, graphene has a long spin-relaxation time and a long spin-diffusion length, which underlies the potential application of graphene in spintronics. A key step for realizing graphene-based spintronic devices is injection of a spin current into graphene, which has been the focus of many studies. The first work on spin transport in graphene was reported in 2006 by Hill *et al.* [2]. Using ferromagnetic (FM) NiFe electrodes, they observe a spin-valve effect, in which a spin-polarized current injected from one ferromagnetic electrode goes through graphene before being detected at the other electrode. This idea was soon pursued by several other groups [3–6]. However, the reported spin-injection efficiency, a key parameter for spin transport, is only about 1% if graphene is directly in contact with the FM leads [2,3,6]. The low spin-injection efficiency is mainly due to a mismatch of spin "conductance" [7–9] between the ferromagnet and graphene. In a typical heterostructure of a ferromagnetic electrode and a nonmagnetic (NM) material such as graphene, spins injected from the electrode into the NM material may diffuse through the NM material or backscatter to the lead [7–9]. The flow of the spin current via diffusion depends on the spin resistance of the NM material as well as matching of the resistances of the two materials at the FM/NM interface [10]. The reported ratio of spin resistance of the ferromagnet (R_{FM}) over that of graphene (R_G) varies from 10^{-3} to 10^{-5} [11]. Because $R_{\mathrm{FM}} \ll R_G$, spin diffusion in a typical FM/graphene junction is dominated by the backscattering of spins into the FM lead, which is the reason for the low spin-injection efficiency [11].

To enhance the spin-injection efficiency, insulating oxides such as Al_2O_3 and MgO are used as a tunnel barrier between the ferromagnetic electrode and graphene [4,5,12–15]. It has been demonstrated that, if the interfacial spin-dependent resistivity can be tuned to the same order of magnitude as the spin-dependent resistivity of graphene, efficient spin injection can be achieved [6]. However, not all systems exhibit perfect barrier effects. Using Al_2O_3 and MgO as a tunnel barrier, respectively, Tombros *et al.* [4] and Han *et al.* [3] separately report a good match of contact resistances but low spin-injection efficiency from a Co electrode to graphene, which is attributed to issues related to the materials and their interface. For example, pinholes are observed in the Al_2O_3 barrier by van Wees's group which may create a short circuit between graphene and the ferromagnetic electrode, resulting in a reduced spin-injection efficiency [4,5]. To reduce pinholes, Dlubak and co-workers recently proposed to use a sputtering technique for sample growth [16]. On the other hand, the formation of clumps of the insulating material on graphene is reported by Kawakami's group which also leads to low spin-injection efficiency. This result is due in part to graphene's reluctance to form strong bonds with

*shenlei@nus.edu.sg
†phyfyp@nus.edu.sg

other materials and can be overcome by incorporating an interfacial TiO_2 layer [11]. Nevertheless, identifying materials with a good conductance match and thus high spin-injection efficiency remains a challenge for graphene-based spintronic applications.

Motivated by recent experimental breakthroughs in synthesizing *h*-BN/graphene heterostructure and the vertical graphene/*h*-BN/graphene field-effect transistor [17–19], here we investigate spin injection from a Ni electrode into graphene with an *h*-BN tunnel barrier, as well as Cu and graphite barriers for comparison. Results of our transport calculations indicate that the insulating *h*-BN tunnel barrier significantly improves the spin-injection efficiency from the Ni lead into graphene. This improvement is possible because of an *h*-BN-induced asymmetry in the spin states of graphene, as revealed by our first-principles electronic structure calculations.

II. MODEL

Graphene was first isolated by mechanical exfoliation from graphite. This method was later applied to other layer-structured materials, creating a family of two-dimensional materials that includes insulating *h*-BN and semiconducting MoS_2 and WS_2, in addition to the semimetallic graphene. These materials can easily form van der Waals structures with well-defined interfacial contact [17,19–24]. In particular, *h*-BN has been demonstrated to be the best candidate for graphene-based heterostructures or sandwich structures because of its wide band gap and the close match of its lattice constant with that of graphene and ferromagnetic Ni [17,24–28]. Good carrier transport and tunneling properties of the graphene/*h*-BN heterostructure or sandwich structures are reported by Geim's group [17,19,21,24]. Furthermore, previous first-principles calculations predict that spin-polarized tunneling can be achieved in Ni(111)/*h*-BN [29–31] and Ni(111)/graphene heterostructures [25–28], as well as Ni(111)/graphene/Ni(111) spin-valve devices [32,33]. Therefore, *h*-BN is selected as a tunnel barrier for spin injection from Ni to graphene. For comparison, we also consider a metallic Cu barrier, as well as a thin graphite layer or a few-layer graphene barrier. Ni(111) is selected as the ferromagnetic source, because it has a similar hexagonal lattice structure as graphene and *h*-BN, and its in-plane lattice constant (2.49 Å) is also close to that of graphene (2.46 Å) and *h*-BN (2.50 Å). The lattice constant of graphene is adopted for the in-plane lattice constant of the Ni(111)/*h*-BN/graphene structure. The small stain induced in Ni(111) and *h*-BN is not expected to make any qualitative difference in the calculated results.

The model used in our study is shown in Fig. 1. Both the left lead (Ni) and the right lead (graphene) are assumed to

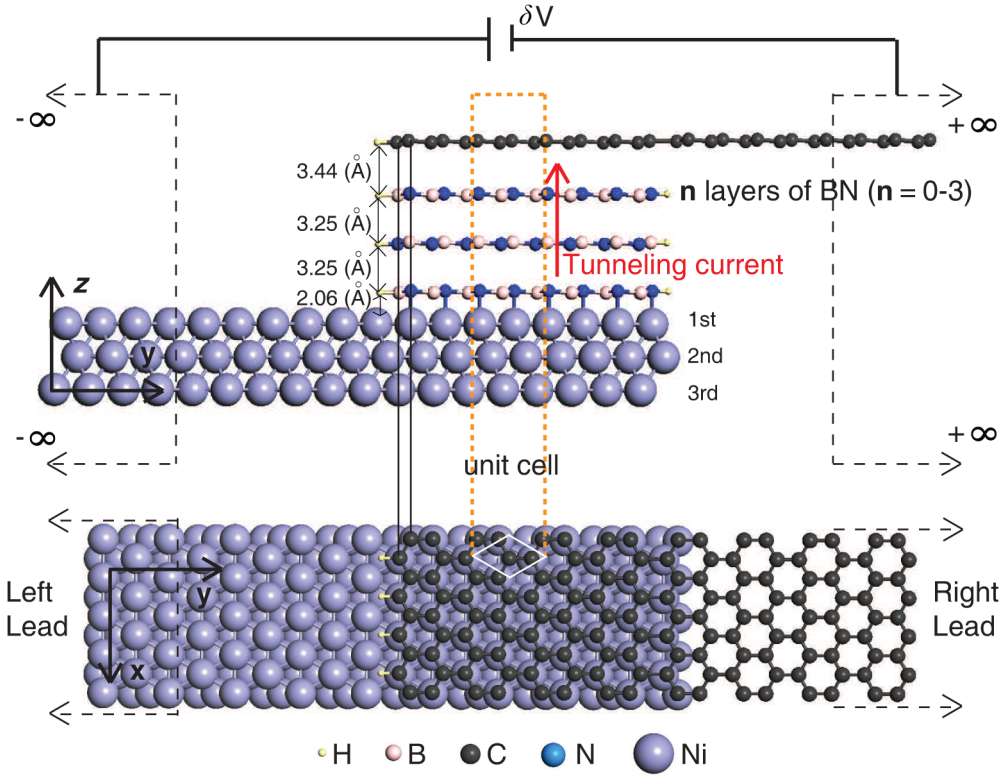

FIG. 1. Side and top views of the Ni(111)/*h*-BN/graphene model. The thickness of the *h*-BN tunnel layer (or Cu, graphite) is varied from 0 (without a tunnel barrier) to 3 atomic layers. The model shown here has three atomic layers of *h*-BN. The supercell used for structural optimization and band structure calculation is indicated by the brown dashed box. The device is built with two semi-infinite leads and a scattering region.

be infinitely long. We also consider a case of $Ni/(h-BN)_3$/graphene with a doubled overlapping area between Ni and BN as well as BN and graphene. We find little change in the spin-injection efficiency. Thus, we use the structure in Fig. 1 in this work. The scattering region or the device consists of the Ni lead at the bottom, the graphene active region at the top, and 0–3 layers of *h*-BN (or Cu, graphene) between them. For convenience of discussion, we assume the transport direction is along the *y* direction and the normal direction of the graphene plane is the *z* direction. The system is periodic along the *x* direction, as shown in Fig. 1. It is noted that a single piece of graphene is used for the active region and the right lead, which would minimize interface scattering between the central region and the right lead in the usual sandwich structures.

A separate slab model, consisting of a monolayer of graphene, six layers of Ni, and 0–3 layers of *h*-BN is used for structural optimization and band structure calculation. During geometry optimization, the bottom four layers of Ni are fixed to their positions in bulk Ni, while all other atoms in the system are allowed to freely relax. In the optimized structure, the distance between the graphene layer and the Ni substrate is 2.04 Å, while the BN-BN and BN-graphene interlayer distances are 3.25 and 3.44 Å, respectively (see Fig. 1), which are in good agreement with results of previous theoretical studies [34]. The BN layer is found to interact strongly with Ni(111). In the optimized structure, the N atom in *h*-BN sits on the top of the Ni atom in the surface layer, forming a N-Ni bond of length 2.06 Å. The B atom in *h*-BN is directly above the Ni atom in the third layer, as shown in Fig. 1. The *A*-*A* stacking is assumed between BN and graphene, because it is the most stable configuration among various possible stackings. The model for transport calculation is constructed from the optimized slab model.

III. COMPUTATIONAL DETAILS

Geometry optimization and electronic structure calculation are carried out by using the density functional theory (DFT) based VASP code [35,36]. The projector-augmented-wave method and the local density approximation (LDA) [37] are adopted to describe the core-valence interactions and the electron exchange and correlation functional. The plane-wave expansion of the electron wave function is cut off at a kinetic energy of 400 eV, and the Brillouin zone of the unit cell is sampled by using a $21 \times 21 \times 1$ *k*-point grid. Structural optimization is carried out until the force on each atom is less than 0.01 eV/Å. The transport properties such as the *I*-*V* curve are studied by using a self-consistent approach that combines DFT and the nonequilibrium Green's function (NEGF) formalism, as implemented in the ATOMISTIX TOOLKIT (ATK) package [38,39], in which the electron transmission used in the Landauer formula is obtained self-consistently for a given value of the bias voltage, the same as in other previous works [32,33,40–42]. The double-ζ-polarized basis set is used to expand the electron wave function in the transport calculation, and a cutoff energy of 150 Ry and a Monkhorst-Pack *k*-point grid of $9 \times 1 \times 100$ yield a good balance between accuracy and computational time. The LDA is also adopted in the transport calculations, and the electron temperature is set to 300 K. A finer *k*-point mesh (201×1) is used to sample the periodic direction perpendicular to the transport direction. A vacuum region of 15 Å is used to separate the device from its periodic image to minimize the artificial interaction between them.

IV. RESULTS AND DISCUSSIONS

A. Transport property

1. Ni(111)/*graphene junction without a tunnel barrier*

Before we examine the effect of a tunnel barrier, we calculate and present here the transport property of the Ni(111)/graphene junction in which graphene is directly in contact with the Ni(111) electrode. The device structure is shown in Fig. 2(a). It is similar to the structure shown in Fig. 1 but without the *h*-BN layers. The calculated transmission spectrum of the Ni(111)/graphene junction under a bias voltage of 0.3 V is shown in Fig. 2(c), where the bias voltage window is within the two vertical dashed lines. As can be seen, the total transmissions of spin-up and spin-down states are similar within the bias voltage window, except a peak near −0.10 eV in the spin-down state. This result implies that the spin polarization of the current passing through the device will not be high if the Ni lead is directly deposited on graphene.

For a more qualitative measure of spin polarization, i.e., spin-injection efficiency from Ni lead into graphene, we calculate the *I*-*V* curves by using the NEGF approach. The spin-resolved current I_σ, where σ indicates the spin-up or spin-down state, is obtained from

$$I_\sigma = \frac{e}{h}\int_{-\infty}^{+\infty} T_\sigma(E,V)[f_L(E,\mu_L) - f_R(E,\mu_R)]dE, \quad (1)$$

where e, h, and T are the electron charge, Planck's constant, and the transmission, respectively. f_L and f_R in the above equation are the Fermi distribution functions of the left and right lead, respectively. Under a bias voltage V, the chemical potentials of the left lead and right lead are shifted to $\mu_L = E_F - eV/2$ and $\mu_R = E_F + eV/2$, respectively. The calculated *I*-*V* curve of the Ni(111)/graphene junction when the bias voltage is varied from 0 to 0.3 V is shown in Fig. 2(b). It is clear that spin-down electrons are the majority spin in the current. The spin-down current is larger than the spin-up current but not overwhelmingly. This transport property can be partially explained by the electronic structure at the Fermi surface of Ni(111) and graphene [28]. When the Fermi surfaces of fcc Ni and

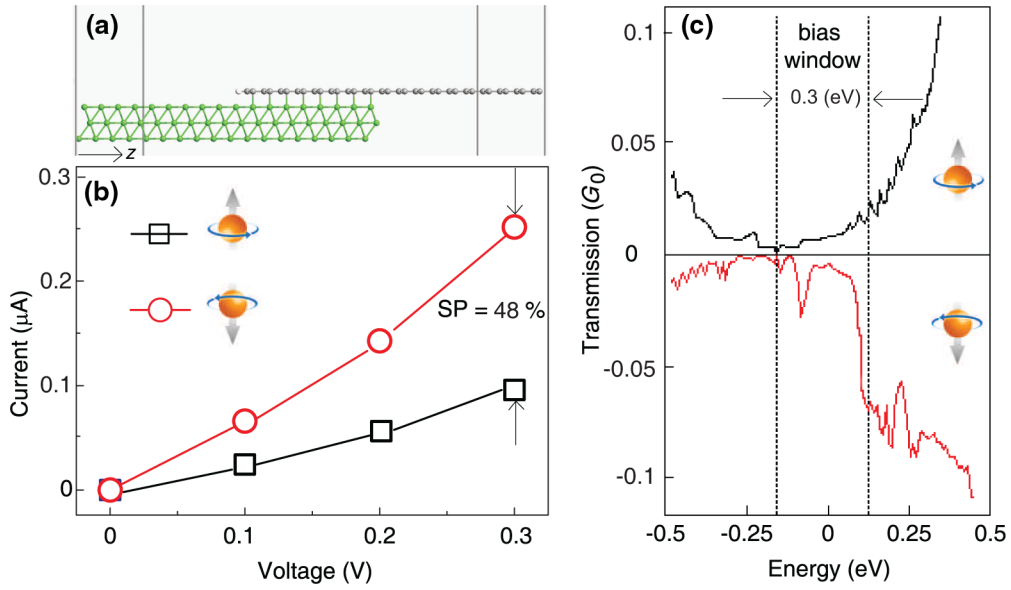

FIG. 2. (a) Model for Ni(111)/graphene. (b) The calculated *I-V* curve of Ni(111)/graphene. (c) The transmission spectrum of Ni(111)/graphene under a bias voltage of 0.3 V.

graphene are projected to the (111) plane, a higher density of states is found for the down spin near the six high-symmetry points (K or K') which are the main transport channels of graphene. In contrast, the Fermi surface states for the up spin of Ni are located elsewhere [28]. Therefore, spin-down electrons dominate over spin-up electrons in the current under a bias voltage [Fig. 2(b)]. The spin-injection efficiency is calculated from $|I_{\mathrm{up}} - I_{\mathrm{down}}|/|I_{\mathrm{up}} + I_{\mathrm{down}}|$. Under a bias voltage of 0.3 V, the estimated spin-injection efficiency of Ni(111)/graphene is 48%. This result, however, is an optimistic value estimated based on an ideal model. Under experimental conditions, this value is expected to be reduced by an interfacial effect such as interfacial disorder [4,5,14,43–45].

2. Ni(111)/*graphene junction with an h-BN tunnel barrier*

Spin tunneling has been proposed as a way of overcoming the conductance mismatch and is widely used to enhance the spin-injection efficiency of spintronic devices, such as silicon-based devices [46]. It is therefore natural to ask whether the same approach works here and can be used to enhance spin-injection efficiency from a FM lead to graphene. To investigate the effect of a tunnel barrier, we insert n ($n = 1, 2, 3$) layers of *h*-BN between Ni(111) and monolayer graphene, as illustrated in Fig. 1. The model used in our transport calculation is also shown in Fig. 3(a). The spin-tunneling transport properties of the Ni(111)/*h*-BN/graphene are calculated, and the results are presented in Fig. 3. As shown in Fig. 3(c), the transmission spectrum of spin-up states under a bias voltage of 0.3 V is greatly suppressed within the bias voltage window, while that of the spin-down states remains significant. The calculated *I-V* curve of the Ni(111)/*h*-BN/graphene device with three layers of *h*-BN [Fig. 3(b)] confirms that the majority-spin current is much larger than the minority-spin current under a bias voltage. The estimated spin-injection efficiency of the Ni(111)/*h*-BN/graphene device with 1–3 layers of *h*-BN is given in Table 1. The results indicate that the spin-injection efficiency from the ferromagnet into graphene can be dramatically enhanced by tunneling through an *h*-BN barrier. With a single layer of *h*-BN, the spin-injection efficiency increases to 72%, which is close to the experimental results of 64% [47] and much higher than 1% of FM/graphene [3] or 30% of FM/oxide/graphene [11]. The maximum spin-injection efficiency (100%) can be achieved with three or more layers of *h*-BN between the FM lead and graphene. The enhancement of the spin-injection efficiency is due to the improvement of the conductance mismatch. Figures 2(b) and 3(b) show the current (I) is reduced from microampere to nanoampere after inserting *h*-BN. It means that the resistance of FM electrodes is increased by *h*-BN barriers around 3 orders of magnitude. Thus, the resistance of R_F and R_G is close, indicating a good conductance match.

To understand how the *h*-BN tunnel barrier affects the spin-up and spin-down currents, we calculate the spin-resolved transmission eigenstates and present the results for the device with three layers of *h*-BN in Fig. 4. For the spin-up states, we can see clearly in Fig. 4(a) that most of the transmission states are localized in the first two layers of *h*-BN from the Ni electrode and a little on the N atoms in the third *h*-BN layer which is next to graphene. The eigenstates in the third *h*-BN layer show clear p characteristics. Therefore, the transport channel of spin-up states of graphene is essentially blocked. On the other hand, the

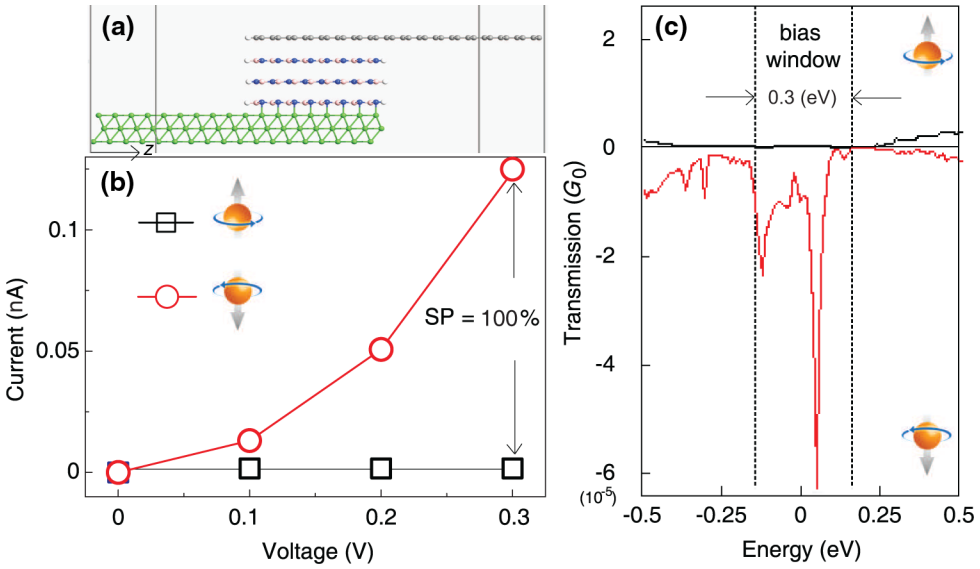

FIG. 3. (a) Model for Ni(111)/(h-BN)$_3$/graphene. The subscript 3 indicates three atomic layers of h-BN. (b) The calculated I-V curve of Ni(111)/(h-BN)$_3$/graphene. (c) The transmission spectrum of Ni(111)/(h-BN)$_3$/graphene under a bias voltage of 0.3 V.

spin-down transmission states are delocalized in all h-BN layers as well as graphene, as shown in Fig. 4(b). The transport channel of the spin-down states of graphene is thus open, and the spin-down electrons can be easily injected from the Ni electrode to graphene. It is noted that the transport channel in graphene is of carbon p_z characteristic [Fig. 4(b)]. Based on the spin-resolved transmission eigenstates of the two transport channels, we present a schematic diagram in Fig. 4(c) to illustrate the effect of the insulating barrier on the electron transport property of the proposed structure. Because of improved conductance matching by using a tunnel barrier [11], the spin-polarized electric current is injected into graphene from a ferromagnetic electrode. The injected electric current is highly spin polarized, because the majority-spin-transport channel is blocked by the tunnel barrier.

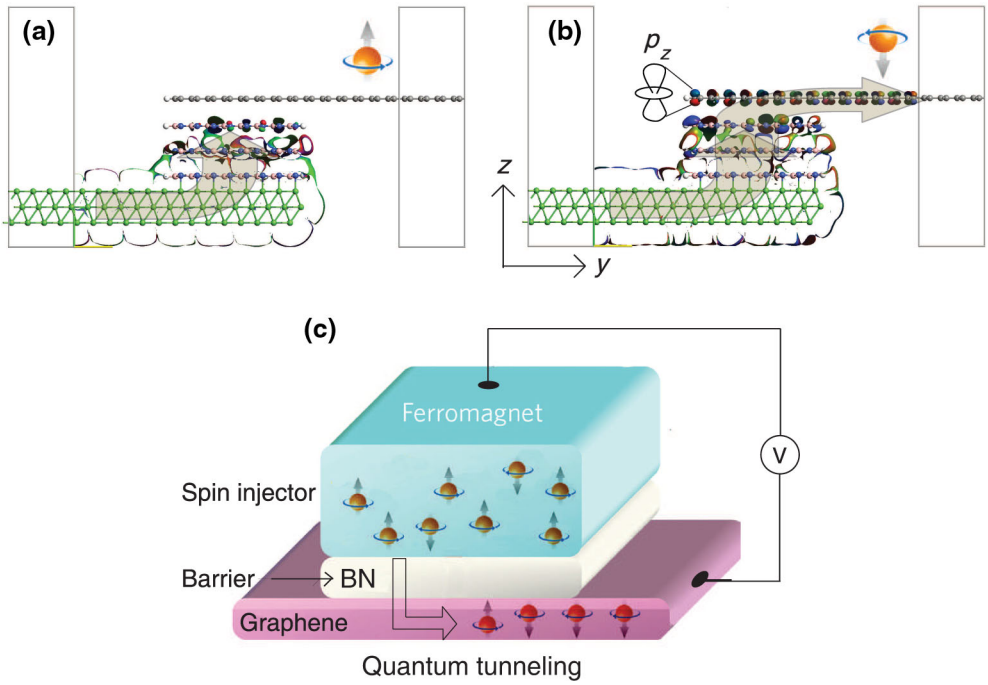

FIG. 4. The calculated spin-resolved transmission eigenstates of (a) the spin-up channel and (b) the spin-down channel of Ni(111)/(h-BN)$_3$/graphene under a bias voltage of 0.3 V. (c) Schematic diagram showing the effect of a tunnel barrier on the spin polarization of a current injected from the Ni(111) electrode to graphene.

3. Ni(111)/*graphene junction with a Cu or graphite barrier*

The Ni(111)/graphene/Ni(111) junction is proposed to have large magnetoresistance (MR) [27,28,32,48]. The MR ratio (pessimistic) can reach 100% if five or more layers of graphene are used. But if a monolayer graphene is sandwiched between the open *d*-shell transition metals, such as Ni, its characteristic electronic structure of topological singularities at the *K* points in the reciprocal space would be destroyed by the formation of strong chemical bonds between graphene and transitional-metal electrodes, leading to a low MR ratio. Karpan *et al.* proposed to insert several layers of inert Cu to avoid bond formation between graphene and metal lead [27]. It is found that, with a single layer of Cu between Ni and graphene, the electronic structure of graphene can be restored and its MR ratio can reach 90%. The MR ratio can be further increased by incorporating more layers of graphene between metal leads [27].

Of course, magnetoresistance is different from the spin-injection ratio. The former relies on the magnetic configuration of the two electrodes and is an extrinsic property of a system, while the spin-injection ratio is determined by the spin-dependent behaviors of injected electrons and is an intrinsic property of the system. Despite this difference, it is interesting to find out whether a Cu or graphite barrier is useful for enhancing the spin-injection efficiency between graphene and the Ni(111) electrode. With this in mind and also to serve as a comparison with the *h*-BN tunnel barrier, we also calculate the spin-injection efficiencies of Ni(111)/graphene junctions with a few atomic layers of Cu(111) or graphite as a barrier in Fig. 5 and list the results in Table 1. It is clear that the spin-injection ratio is low with either graphite or Cu(111) as the barrier. The reason is because a few layers of graphite or Cu are metallic. The lack of tunneling effect makes the metallic barriers less effective in overcoming the conductance mismatch between Ni and graphene, compared to an insulating barrier such as *h*-BN. Experimentally, it is demonstrated that a thin titanium seed layer between TM electrodes and graphene improves the contact conductivity and lattice match but does not lead to enhancement in the spin-injection ratio [11], due to the same reason. Nevertheless, based on the results of our calculations, a good spin-injection ratio (79%) may be achieved if a monolayer of Cu(111) is inserted between the Ni(111) electrode and graphene. This result is because the Cu layer weakens the interaction between Ni and graphene, allowing the graphene to recover its characteristic electronic property. However, since Cu is metallic, electron transport through Cu is not by tunneling. If the thickness of the Cu barrier is more than one atomic layer, the spin-injection ratio is hampered by the conductance mismatch between Cu and graphene. By comparing the performances of the three different barriers (Table 1), it is obvious that the insulating *h*-BN, which interacts with

TABLE I. The calculated spin-injection efficiency of Ni(111)/barrier/graphene under a bias voltage of 0.3 V. Three different barriers, *h*-BN, graphene, and Cu (111), of different thickness (1, 2, or 3 atomic layers, L) are considered.

	Spin-injection efficiency		
Barrier	1L	2L	3L
h-BN	72%	96%	100%
Graphene	29%	31%	24%
Cu(111)	79%	12%	13%

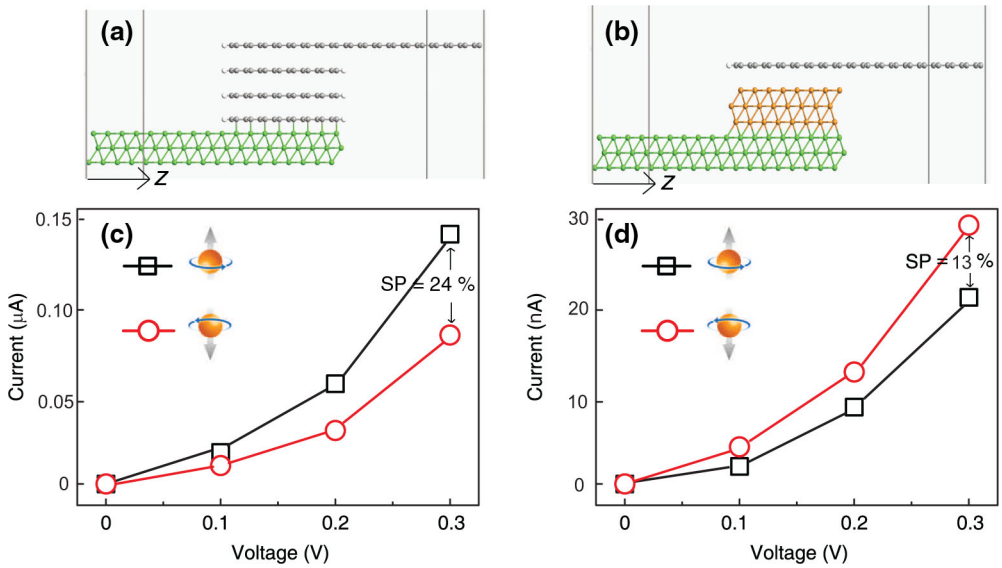

FIG. 5. Models for (a) Ni(111)/$(\text{graphite})_3$/graphene and (b) Ni(111)/$(\text{Cu})_3$/graphene. The subscript indicates the thickness of the barrier in the number of atomic layers. (c),(d) The calculated *I*-*V* curves of the above two devices, respectively.

graphene through the van der Waals force, is the most promising barrier to facilitate spin injection from a FM electrode into graphene, for graphene-based spintronic applications.

B. Electronic structures

1. Band structures

From the results of our transport calculations presented above, we know that the *h*-BN tunnel barrier is effective in promoting spin injection from a TM electrode into graphene. In order to understand the underlying physics, we calculate the spin-resolved band structure and local density of states of the Ni(111)/*h*-BN/graphene structures. The results obtained for the structure with a single layer of *h*-BN between Ni (111) and graphene are shown in Fig. 6, along with those without an *h*-BN barrier for comparison. The solid circles in Fig. 6 represent the weight of the graphene-derived p_z orbital. We pay attention to the graphene-derived p_z orbital, because it is the main transport channel as shown in Fig. 4(b). As shown in Figs. 6(a) and 6(b), when the Ni electrode is in direct contact with graphene, a band gap of about 0.34 eV opens in both spin-up and spin-down bands of graphene, which is in agreement with results of previous experiments and calculations [27,31,49]. The gap opening is due to a strong interaction between graphene and Ni. The similar band structures for majority and minority carriers imply a low spin-injection efficiency if the ferromagnetic Ni lead is directly deposited on graphene. In fact, because of the conductance mismatch between Ni and graphene ($R_{\mathrm{Ni}}/R_{\mathrm{graphene}}$ ranges from 10^{-3} to 10^{-5}) [11], most of the charge carriers would be backscattered to Ni at the Ni/graphene interface. Moreover, the measured spin polarization can be further reduced by the interfacial effect and/or interfacial disorder in experimentally grown samples [50,51]. All of these result in a much lower spin-injection efficiency into graphene [4,5,14]. Interestingly, when a layer of *h*-BN is incorporated between Ni and graphene, a band gap of about 85 meV opens in the spin-up bands of graphene, while the spin-down bands remain gapless, as shown in Figs. 6(c) and 6(d). In other words, the semimetallic characteristics of graphene are restored in the spin-down states by the *h*-BN layer. It is this *h*-BN-induced imbalance between the two spin states of graphene that results in the significantly different transport performance of the two spin channels. This imbalance is the root of the high spin-injection efficiency of the Ni(111)/*h*-BN/graphene device.

2. Local density of states

To understand why an *h*-BN layer induces asymmetric effects on the two spin states of graphene, we examine the local density of states (LDOS) projected on the relevant atoms and orbitals. As can be seen in Fig. 7(a), there exists

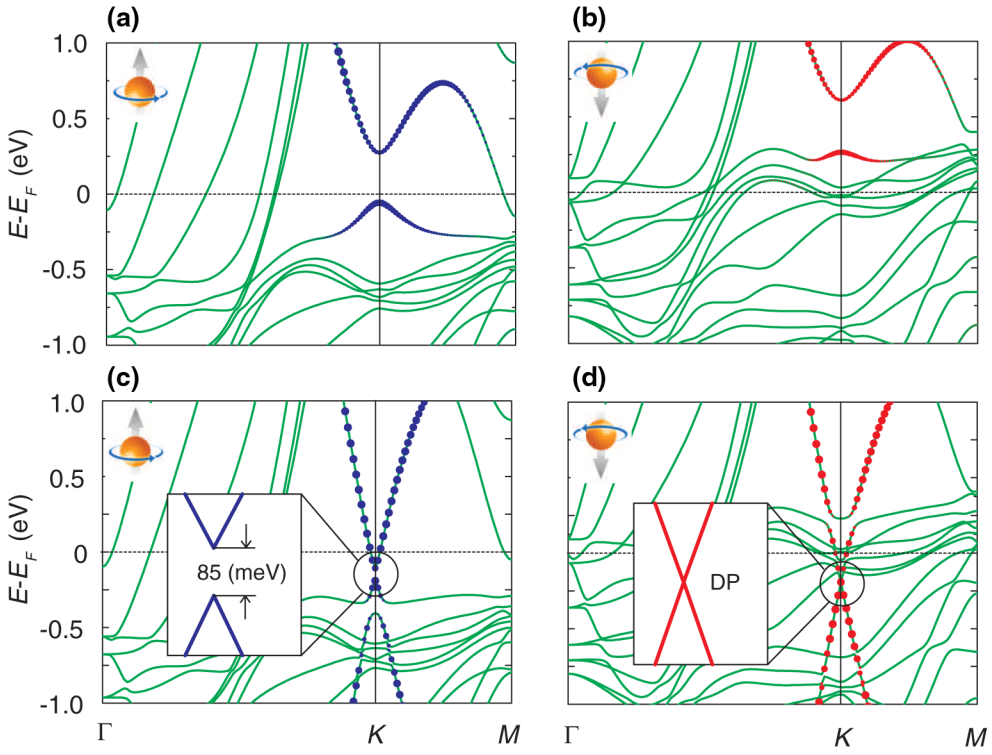

FIG. 6. Spin-resolved band structures of Ni(111)/graphene without a tunnel barrier (upper panels) and with one atomic layer of *h*-BN (lower panels), respectively. The spin-up (-down) band structure is shown in the left (right) panel, in each case. The solid circles represent the weight of the graphene-derived p_z orbital.

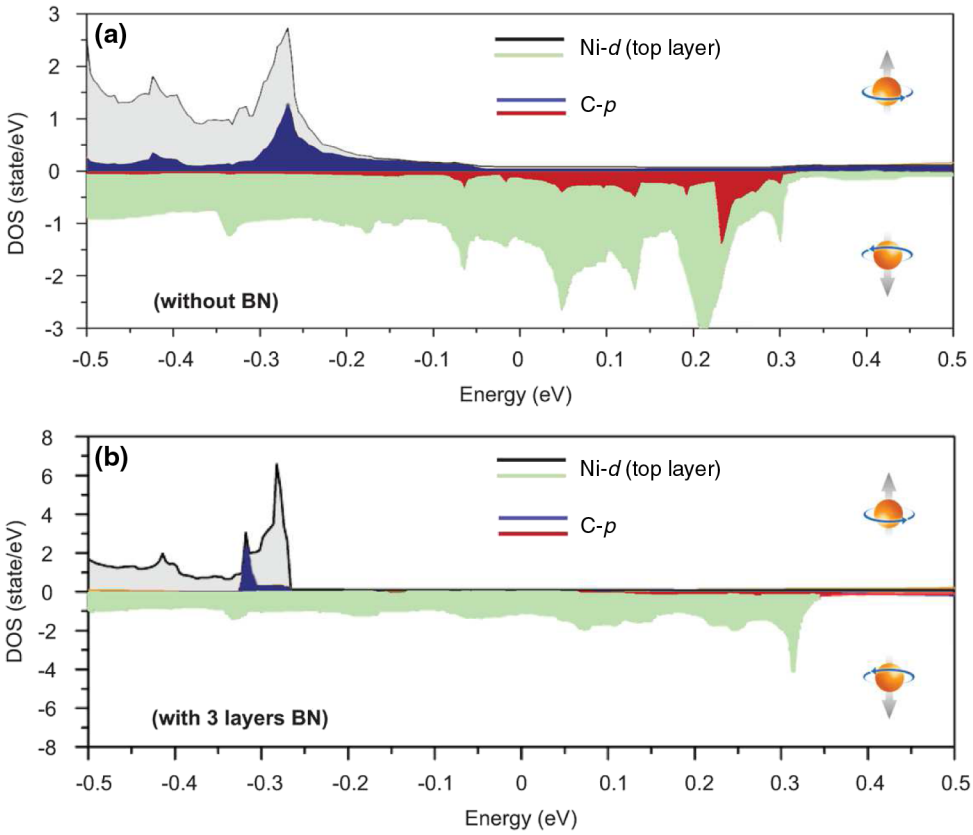

FIG. 7. LDOS of Ni(111)/graphene (a) without a tunnel barrier and (b) with one atomic layer of *h*-BN, respectively. The LDOS on B and N orbitals are not shown. To show the details, the LDOS of C p are enlarged by 5 times. As can be seen, the overlap of spin-down states of C p and Ni d disappears after inserting *h*-BN.

a strong overlap between the C p and Ni d orbitals in both spin-up states, in the energy range of −0.23 to −0.3 eV, and spin-down states, between 0.23 and 0.28 eV, if metallic Ni is in direct contact with graphene. When one atomic layer of *h*-BN is incorporated between Ni and graphene, the interaction between the C p and Ni d orbitals is eliminated in the spin-down states, as shown in Fig. 7(b). However, a weak coupling between these orbitals still exists in the spin-up states, in the energy range of −0.3 to −0.32 eV. Further examination of the projected density of states (PDOS) of other atoms reveals that this weak coupling is mediated by the N p_z orbitals (not shown here). These features in the PDOS of the concerned atoms and the close relationship between DOS and transmission lend further support that Ni/*h*-BN/graphene is an efficient tunneling barrier interface.

V. CONCLUSIONS

The issue of spin-conductance mismatch and resulting low spin-injection efficiency which hampers the practical application of graphene in spintronics is addressed by using first-principles electronic structure and transport calculations. *h*-BN is found to be an effective tunnel barrier for enhancing the spin-current injection efficiency from ferromagnetic electrodes into graphene. Our study suggests that tunneling transport can efficiently overcome the spin-conductance mismatch between ferromagnetic electrodes and graphene, similar to other channel materials. Recently, Yamaguchi *et al.* demonstrated spin injection into bilayer graphene from ferromagnetic $Ni_{0.8}Fe_{0.2}$ electrodes through a single-crystal monolayer *h*-BN [47]. These studies pave the way for spintronic devices based on graphene as well as other 2D materials. Note that two-terminal devices should require more considerations besides the spin-injection efficiency but will need to be treated along the guidelines in Refs. [7–9].

ACKNOWLEDGMENTS

The authors thank S. C. Li and P. J. Kelly for their helpful comments on the discussion of Cu(111) and graphite barriers and asymmetric characteristics of two spin states of graphene with the *h*-BN barrier. This work is partially supported by A*STAR (Agency for Science, Technology and Research, Singapore) Research Funding (Grant No. 092-156-0121).

[1] A. K. Geim and K. S. Novoselov, The rise of graphene, Nat. Mater. **6**, 183 (2007).

[2] E. W. Hill, A. K. Geim, K. Novoselov, F. Schedin, and P. Blake, Graphene spin valve devices, IEEE Trans. Magn. **42**, 2694 (2006).

[3] W. Han, K. Pi, W. Bao, K. M. McCreary, Y. Li, W. H. Wang, C. N. Lau, and R. K. Kawakami, Electrical detection of spin precession in single layer graphene spin valves with transparent contacts, Appl. Phys. Lett. **94**, 222109 (2009).

[4] N. Tombros, C. Jozsa, M. Popinciuc, H. T. Jonkman, and B. J. van Wees, Electronic spin transport and spin precession in single graphene layers at room temperature, Nature (London) **448**, 571 (2007).

[5] M. Popinciuc, C. Jozsa, P. J. Zomer, N. Tombros, A. Veligura, H. T. Jonkman, and B. J. van Wees, Electronic spin transport in graphene field-effect transistors, Phys. Rev. B **80**, 214427 (2009).

[6] H. Goto, A. Kanda, T. Sato, S. Tanaka, Y. Ootuka, S. Odaka, H. Miyazaki, K. Tsukagoshi, and Y. Aoyagi, Gate control of spin transport in multilayer graphene, Appl. Phys. Lett. **92**, 212110 (2008).

[7] G. Schmidt, D. Ferrand, L. W. Molenkamp, A. T. Filip, and B. J. van Wees, Fundamental obstacle for electrical spin injection from a ferromagnetic metal into a diffusive semiconductor, Phys. Rev. B **62**, R4790 (2000).

[8] E. I. Rashba, Theory of electrical spin injection: Tunnel contacts as a solution of the conductivity mismatch problem, Phys. Rev. B **62**, R16267 (2000).

[9] A. Fert and H. Jaffres, Conditions for efficient spin injection from a ferromagnetic metal into a semiconductor, Phys. Rev. B **64**, 184420 (2001).

[10] S. Takahashi and S. Maekawa, Spin injection and detection in magnetic nanostructures, Phys. Rev. B **67**, 052409 (2003).

[11] W. Han, K. Pi, K. M. McCreary, Y. Li, J. J. I. Wong, A. G. Swartz, and R. K. Kawakami, Tunneling spin injection into single layer graphene, Phys. Rev. Lett. **105**, 167202 (2010).

[12] B. Dlubak, P. Seneor, A. Anane, C. Barraud, C. Deranlot, D. Deneuve, B. Servet, R. Mattana, F. Petroff, and A. Fert, Are Al_2O_3 and MgO tunnel barriers suitable for spin injection in graphene?, Appl. Phys. Lett. **97**, 092502 (2010).

[13] C. Józsa, M. Popinciuc, N. Tombros, H. T. Jonkman, and B. J. van Wees, Electronic spin drift in graphene field-effect transistors, Phys. Rev. Lett. **100**, 236603 (2008).

[14] C. Józsa, M. Popinciuc, N. Tombros, H. T. Jonkman, and B. J. van Wees, Controlling the efficiency of spin injection into graphene by carrier drift, Phys. Rev. B **79**, 081402 (2009).

[15] C. Józsa, T. Maassen, M. Popinciuc, P. J. Zomer, A. Veligura, H. T. Jonkman, and B. J. van Wees, Linear scaling between momentum and spin scattering in graphene, Phys. Rev. B **80**, 241403 (2009).

[16] B. Dlubak, M.-B. Martin, C. Deranlot, K. Bouzehouane, S. Fusil, R. Mattana, F. Petroff, A. Anane, P. Seneor, and A. Fert, Homogeneous pinhole free 1 nm Al_2O_3 tunnel barriers on graphene, Appl. Phys. Lett. **101**, 203104 (2012).

[17] L. Britnell, R. V. Gorbachev, R. Jalil, B. D. Belle, F. Schedin, A. Mishchenko, T. Georgiou, M. I. Katsnelson, L Eaves, S. V. Morozov, N. M. R. Peres, J. Leist, A. K. Geim, K. S. Novoselov, and L. A. Ponomarenko, Field-effect tunneling transistor based on vertical graphene heterostructures, Science **335**, 947 (2012).

[18] S. Roth, F. Matsui, T. Greber, and J. Osterwalder, Chemical vapor deposition and characterization of aligned and incommensurate graphene/hexagonal boron nitride heterostack on Cu (111), Nano Lett. **13**, 2668 (2013).

[19] S. J. Haigh, A. Gholinia, R. Jalil, S. Romani, L. Britnell, D. C. Elias, K. S. Novoselov, L. A. Ponomarenko, A. K. Geim, and R. Gorbachev, Cross-sectional imaging of individual layers and buried interfaces of graphene-based heterostructures and superlattices, Nat. Mater. **11**, 764 (2012).

[20] L. Britnell, R. V. Gorbachev, R. Jalil, B. D. Belle, F. Schedin, M. I. Katsnelson, L. Eaves, S. V. Morozov, A. S. Mayorov, N. M. R. Peres, A. H. Castro Neto, J. Leist, A. K. Geim, L. A. Ponomarenko, and K. S. Novoselov, Electron tunneling through ultrathin boron nitride crystalline barriers, Nano Lett. **12**, 1707 (2012).

[21] T. Georgiou, R. Jalil, B. D. Belle, L. Britnell, R. V. Gorbachev, S. V. Morozov, Y.-J. Kim, A. Gholinia, S. J. Haigh, O. Makarovsky, L. Eaves, L. A. Ponomarenko, A. K. Geim, K. S. Novoselov, and A. Mishchenko, Vertical field-effect transistor based on graphene-WS_2 heterostructures for flexible and transparent electronics, Nat. Nanotechnol. **8**, 100 (2013).

[22] M. S. Choi, G.-H. Lee, Y.-J. Yu, D.-Y. Lee, S. H. Lee, P. Kim, J. Hone, and W. J. Yoo, Controlled charge trapping by molybdenum disulphide and graphene in ultrathin heterostructured memory devices, Nat. Commun. **4**, 1624 (2013).

[23] W. J. Yu, Z. Li, H. Zhou, Y. Chen, Y. Wang, Y. Huang, and X. Duan, Vertically stacked multi-heterostructures of layered materials for logic transistors and complementary inverters, Nat. Mater. **12**, 246 (2012).

[24] A. K. Geim and I. V. Grigorieva, Van der Waals heterostructures, Nature (London) **499**, 419 (2013).

[25] H. Liu, H. Kondo, and T. Ohno, Contact effects of nickel and copper on electron transport through graphene, Phys. Rev. B **86**, 155434 (2012).

[26] J. Maassen, W. Ji, and H. Guo, Graphene spintronics: The role of ferromagnetic electrodes, Nano Lett. **11**, 151 (2011).

[27] V. M. Karpan, P. A. Khomyakov, A. A. Starikov, G. Giovannetti, M. Zwierzycki, M. Talanana, G. Brocks, J. Van Den Brink, and P. J. Kelly, Theoretical prediction of perfect spin filtering at interfaces between close-packed surfaces of Ni or Co and graphite or graphene, Phys. Rev. B **78**, 195419 (2008).

[28] V. M. Karpan, G. Giovannetti, P. A. Khomyakov, M. Talanana, A. A. Starikov, M. Zwierzycki, J. Van Den Brink, G. Brocks, and P. J. Kelly, Graphite and graphene as perfect spin filters, Phys. Rev. Lett. **99**, 176602 (2007).

[29] O. V. Yazyev and A. Pasquarello, Magnetoresistive junctions based on epitaxial graphene and hexagonal boron nitride, Phys. Rev. B **80**, 035408 (2009).

[30] V. M. Karpan, P. A. Khomyakov, G. Giovannetti, A. A. Starikov, and P. J. Kelly, Ni(111)|graphene|*h*-BN junctions as ideal spin injectors, Phys. Rev. B **84**, 153406 (2011).

[31] G. Giovannetti, P. A. Khomyakov, G. Brocks, P. J. Kelly, and J. van den Brink, Substrate-induced band gap in

graphene on hexagonal boron nitride: Ab initio density functional calculations, Phys. Rev. B **76**, 073103 (2007).
[32] K. K. Saha, A. Blom, K. S. Thygesen, and B. K. Nikolić, Magnetoresistance and negative differential resistance in Ni/graphene/Ni vertical heterostructures driven by finite bias voltage: A first-principles study, Phys. Rev. B **85**, 184426 (2012).
[33] Y. Cho, Y. C. Choi, and K. S. Kim, Graphene spin-valve device grown epitaxially on the Ni(111) substrate: A first principles study, J. Phys. Chem. C **115**, 6019 (2011).
[34] P. V. Avramov, A. A. Kuzubov, S. Sakai, M. Ohtomo, S. Entani, Y. Matsumoto, H. Naramoto, and N. S. Eleseeva, Contact-induced spin polarization in graphene/*h*-BN/Ni nanocomposites, J. Appl. Phys. **112**, 114303 (2012).
[35] G. Kresse and J. Furthmüller, Efficient iterative schemes for ab initio total-energy calculations using a plane-wave basis set, Phys. Rev. B **54**, 11169 (1996).
[36] G. Kresse and J. Furthmuller, Efficiency of ab-initio total energy calculations for metals and semiconductors using a plane-wave basis set, Comput. Mater. Sci. **6**, 15 (1996).
[37] J. P. Perdew and A. Zunger, Self-interaction correction to density-functional approximations for many-electron systems, Phys. Rev. B **23**, 5048 (1981).
[38] M. Brandbyge, J.-L. Mozos, P. Ordejón, J. Taylor, and K. Stokbro, Density-functional method for nonequilibrium electron transport, Phys. Rev. B **65**, 165401 (2002).
[39] J. Taylor, H. Guo, and J. Wang, Ab initio modeling of quantum transport properties of molecular electronic devices, Phys. Rev. B **63**, 245407 (2001).
[40] L. Shen, M. Zeng, S. Li, M. B. Sullivan, and Y. P. Feng, Electron transmission modes in electrically biased graphene nanoribbons and their effects on device performance, Phys. Rev. B **86**, 115419 (2012).
[41] L. Shen, T. Zhou, Z. Bai, M. Zeng, J. Q. Goh, Z.-M. Yuan, G. Han, B. Liu, and Y. P. Feng, Systematic study of ferroelectric, interfacial, oxidative, and doping effects on conductance of $Pt/BaTiO_3/Pt$ ferroelectic tunnel junctions, Phys. Rev. B **85**, 064105 (2012).
[42] Z. Bai, L. Shen, Q. Wu, M. Zeng, J.-S. Wang, G. Han, and Y. P. Feng, Boron diffusion induced symmetry reduction and scattering in CoFeB/MgO/CoFeB magnetic tunnel junctions, Phys. Rev. B **87**, 014114 (2013).
[43] E. N. Voloshina, A. Generalov, M. Weser, S. Böttcher, K. Horn, and Y. S. Dedkov, Structural and electronic properties of the graphene/Al/Ni(111) intercalation system, New J. Phys. **13**, 113028 (2011).
[44] C. Zhang, Y. Wang, B. Wu, and Y. Wu, The effect of a copper interfacial layer on spin injection from ferromagnet to graphene, Appl. Phys. A **111**, 339 (2013).
[45] C. Zhang, Y. Wang, B. Wu, and Y. Wu, Enhancement of spin injection from ferromagnet to graphene with a Cu interfacial layer, Appl. Phys. Lett. **101**, 022406 (2012).
[46] R. Jansen, Silicon spintronics, Nat. Mater. **11**, 400 (2012).
[47] T. Yamaguchi, Y. Inoue, S. Masubuchi, S. Morikawa, M. Onuki, K. Watanabe, T. Taniguchi, R. Moriya, and T. Machida, Electrical spin injection into graphene through monolayer hexagonal boron nitride, Appl. Phys. Express **6**, 073001 (2013).
[48] G. Giovannetti, P. A. Khomyakov, G. Brocks, V. M. Karpan, J. Van den Brink, and P. J. Kelly, Doping graphene with metal contacts, Phys. Rev. Lett. **101**, 026803 (2008).
[49] S. Y. Zhou, G.-H. Gweon, A. V. Fedorov, P. N. First, W. A. De Heer, D.-H. Lee, F. Guinea, A. H. Castro Neto, and A. Lanzara, Substrate-induced bandgap opening in epitaxial graphene, Nat. Mater. **6**, 770 (2007).
[50] Y. Ke, K. Xia, and H. Guo, Disorder scattering in magnetic tunnel junctions: Theory of nonequilibrium vertex correction, Phys. Rev. Lett. **100**, 166805 (2008).
[51] Y. Ke, K. Xia, and H. Guo, Oxygen vacancy-induced diffusion scattering, Phys. Rev. Lett. **105**, 236801 (2010).